PHYSICAL REVIEW VOLUME 173, NUMBER 5 25 SEPTEMBER 1968

Study of the Λ-N System in Low-Energy Λ-p Elastic Scattering

G. ALEXANDER, U. KARSHON, A. SHAPIRA, AND G. YEKUTIELI
Nuclear Physics Department, The Weizmann Institute of Science, Rehovoth, Israel

AND

R. ENGELMANN, H. FILTHUTH, AND W. LUGHOFER
Institute for High Energy Physics, Heidelberg University, Heidelberg, Germany

(Received 6 May 1968; revised manuscript received 5 June 1968)

The present paper is based on 378 Λ-p elastic scattering events in the incident-momentum region 120–320 MeV/c. Differential and total cross sections have been measured in several momentum intervals and found to be consistent with predominantly S-wave scattering. No significant indication for the existence of a low-energy Λ-p resonance has been found. Using the effective-range approximation, the four scattering parameters a_s, a_t, r_s, and r_t were evaluated with and without further assumptions on the Λ-p interaction properties. Best values obtained from the four-parameter fit were $a_s=-1.8$, $a_t=-1.6$, $r_s=2.8$, and $r_t=3.3$ F. A likelihood-function mapping procedure is used to describe the large and strongly correlated errors of these values.

I. INTRODUCTION

UNTIL recently most of the information on the hyperon-nucleon (Y-N) interaction has been derived from the analysis of hypernuclei. The main conclusions of this analysis were that the Λ-N potential is spin-dependent, with the singlet interaction stronger than the triplet one, and both interactions being attractive.[1] It is of considerable interest to test these conclusions and to try to obtain additional information on the Y-N system through free Y-N scattering experiments.[2] In particular, from a low-energy Λ-proton interaction experiment, the scattering parameters of the effective-range theory may be directly evaluated and then compared to the values obtained from hypernuclei data through complicated calculations under various assumptions. This paper describes a comprehensive Λ-p elastic scattering experiment in the incident momentum region 120–320 MeV/c. Partial results based on a fraction of the number of events presented here were reported elsewhere.[3–5]

In Sec. II a description of the general experimental procedure is presented and the differential and total Λ-p cross sections are evaluated at different incident-momentum intervals. The S-wave characteristics of the elastic scattering are then used in Sec. III for the evaluation of the scattering parameters using the effective-range formalism with and without further assumptions on the nature of the interaction. In Sec. IV the experimental results are compared with other existing information on Λ-N interactions. Finally, the discrepancy which seems to exist between our best scattering parameters and those obtained from hypernuclei is discussed and arguments in favor of the existence of a hard core in the Λ-N potential are given.

II. EXPERIMENTAL PROCEDURE AND RESULTS

The experiment was carried out on ~200 000 pictures taken at the 81-cm hydrogen bubble chamber exposed to a secondary stopping K^- beam at CERN.[6] The Λ beam was subsequently generated via the K^--p interactions listed in Table I. The search for Λ-$p\to\Lambda$-p events has been performed by a careful scan for V^0 events associated with a recoil proton. Since the reliability of this experiment lies primarily in the detection efficiency of the often short recoil proton and of V^0

TABLE I. Momentum spectrum of a Λ beam produced in K^-p interactions at rest.

K^-p reaction at rest	Branching ratio	Secondary reaction	Hyperon momentum range (MeV/c)	Useful hyperon momentum range (MeV/c)
$K^-p\to\Lambda\pi^0$	0.06	$\cdots$	254.4	254.4
$K^-p\to\Sigma^0\pi^0$	0.28	$\Sigma^0\to\Lambda\gamma$	95.5–244.7	120–244.7
$K^-p\to\Sigma^-\pi^+$	0.45	$\Sigma^-p\to\Lambda n$	289.4[a]	289.4[a]
$K^-p\to\Sigma^-\pi^+$		$\Sigma^-p\to\Sigma^0n$, $\Sigma^0\to\Lambda\gamma$	25.4–130.9[a]	120–130.9[a]

[a] For Σ^- interaction at rest.

[1] R. H. Dalitz, *Nuclear Interactions of the Hyperons* (Oxford University Press, New York, 1965); in the Proceedings of the Conference on the Use of Elementary Particles in Nuclear Structure Research, Brussels, 1965 (unpublished); and references therein.

[2] For a recent summary on hyperon-nucleon scattering experiments and final-state interactions of the Y-N system, see G. Alexander and U. Karshon, in *Proceedings of the Second International Conference on High-Energy Physics and Nuclear Structure, Rehovoth, February, 1967*, edited by G. Alexander (North-Holland Publishing Co., Amsterdam, 1967), p. 36.

[3] B. Sechi-Zorn, R. A. Burnstein, T. B. Day, B. Kehoe, G. A. Snow, G. Alexander, U. Karshon, A. Shapira, G. Yekutieli, R. Engelmann, H. Filthuth, A. Fridman, and A. Minguzzi-Ranzi, in *Proceedings of the Twelfth International Conference on High-Energy Physics, Dubna, 1964* (Atomizdat, Moscow, 1965), p. 675.

[4] G. Alexander, U. Karshon, A. Shapira, G. Yekutieli, R. Engelmann, H. Filthuth, A. Fridman, and A. Minguzzi-Ranzi, Phys. Rev. Letters **13**, 484 (1964).

[5] G. Alexander, O. Benary, U. Karshon, A. Shapira, G. Yekutieli, R. Engelmann, H. Filthuth, A. Fridman, and B. Schiby, Phys. Letters **19**, 715 (1966).

[6] B. Aubert, H. Courant, H. Filthuth, A. Segar, and W. Willis, in *Proceedings of the International Conference on Instrumentation for High-Energy Physics at CERN* (North-Holland Publishing Co., Amsterdam, 1963).

decay events occurring near the production point, special precautions have been taken in order to assure the maximum scanning efficiency. To this end the whole film was scanned twice on three views, and for additional checks part of the film has been scanned a third time. During the scan every suspected V^0 event found within a predetermined fiducial volume was recorded and its neighborhood carefully searched for a possible recoil proton. Following this scanning procedure and after introduction of acceptance criteria which will be described later, an over-all efficiency of 98 and 97% was found for the nonscattered and scattered Λ-decay events.

A. Monitor Events

For the study of the Λ-beam characteristics and for the calculation of the total Λ pathlength examined in this experiment, a random sample of 3129 nonscattered V^0 events lying in the given fiducial volume was measured and identified via the CERN programs THRESH and GRIND. A complete separation between K^0 and Λ decay events was readily obtained by the fitting procedure and by ionization estimation of the tracks on the film.

For the purpose of collecting Λ monitor events of high detection efficiency, we have imposed on the final accepted sample of events four cutoff criteria:

(a) Incoming Λ momentum in the region 120–320 MeV/c (see Fig. 1).

(b) A lower cutoff $L_d = 1.5$ mm in space on the length of the Λ decay proton. This cutoff value was chosen by comparing the experimental proton momentum distribution with the expected one calculated from the experimental Λ-momentum distribution and from the isotropic decay of the proton in the Λ c.m. system (Fig. 2).

(c) A lower cutoff $L_0 = 1.0$ mm in space on the Λ neutral pathlength between the production and the decay points. This cutoff value was derived from the study of the Λ time-of-flight distribution compared with

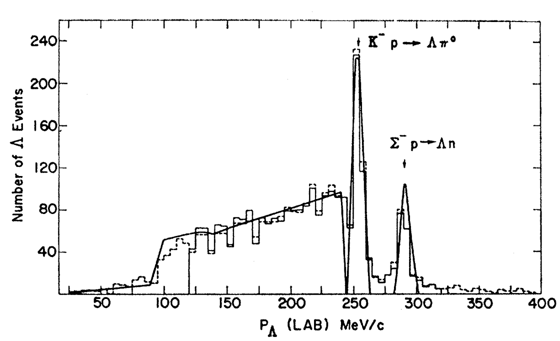

FIG. 1. Momentum distribution of the Λ monitor events before imposing cutoff criteria (dashed line) compared to the expected distribution calculated from K^-p reactions at rest. The solid histogram is the weighted momentum distribution of the Λ monitor events after imposing the cutoff criteria.

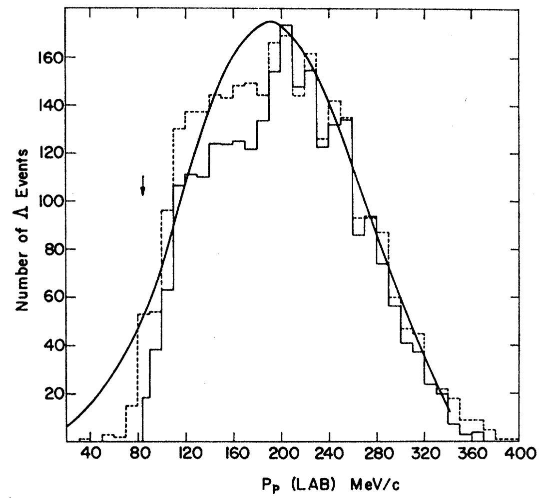

FIG. 2. Momentum distribution of the decaying proton of the monitor events before imposing cutoffs (dashed line) compared to the expected distribution normalized to the same number of events. The solid-line histogram is the weighted momentum distribution of the Λ-decay protons after imposing the cutoff criteria. The arrow represents the lower-momentum cutoff in the decaying proton corresponding to the length cutoff $L_d = 1.5$ mm.

the expected one from a Λ lifetime value[7] of 2.45×10^{-10} sec (Fig. 3).

(d) An upper cutoff $\sin\lambda = 0.98$ was imposed on all dip angles λ of the charged and neutral tracks, since it

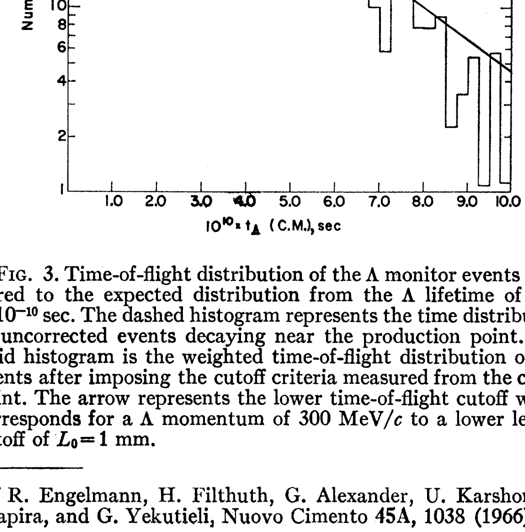

FIG. 3. Time-of-flight distribution of the Λ monitor events compared to the expected distribution from the Λ lifetime of 2.45×10^{-10} sec. The dashed histogram represents the time distribution of uncorrected events decaying near the production point. The solid histogram is the weighted time-of-flight distribution of the events after imposing the cutoff criteria measured from the cutoff point. The arrow represents the lower time-of-flight cutoff which corresponds for a Λ momentum of 300 MeV/c to a lower length cutoff of $L_0 = 1$ mm.

[7] R. Engelmann, H. Filthuth, G. Alexander, U. Karshon, A. Shapira, and G. Yekutieli, Nuovo Cimento 45A, 1038 (1966).

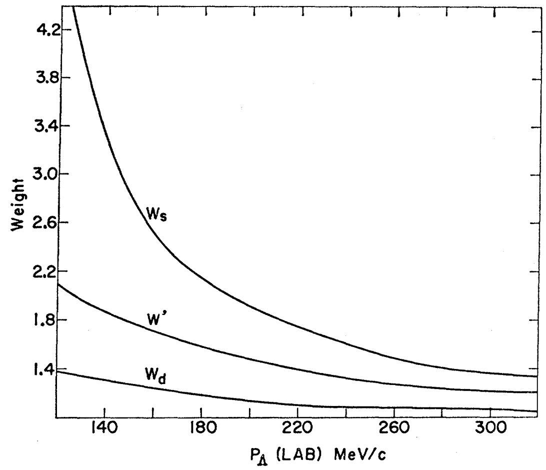

FIG. 4. Average weight of Λ-monitor events (W_d) and of Λ scattering events (W', W_s) as function of the Λ incoming momentum. W_s and W' are average weights for a scattering event with and without correction for the loss of small recoil protons.

was difficult to measure and fit events having tracks with a larger dip angle.

The alternative method of applying cutoffs (b) and (c) on the projected film plane was found to yield approximately the same experimental results. This fact is not surprising since the scan has been carried out simultaneously on all three projected views. Taking into account these cutoff criteria and the fiducial volume restriction, a weight W_d was assigned to each decay event:

$$W_d = W(1)\times W(2)\times W(3) = [P(1)\times P(2)\times P(3)]^{-1},$$

where $P(1)$, $P(2)$, and $P(3)$ are the probabilities for the event to satisfy the cutoff criteria (b), (c), and (d), respectively.[8] Weighted distributions of the Λ momentum, the decaying protons momentum, and the Λ time of flight after imposing the cutoff criteria (a)-(d) are shown in the solid histograms of Figs. 1–3, respectively. The depletion of weighted events in the lower-momentum region in Fig. 2 relative to the uncorrected sample is mainly due to the lower cutoff in the Λ momentum (120 MeV/c). The average weight per event as a function of the Λ momentum calculated from 2213 finally accepted Λ monitor events is shown in Fig. 4. The Λ momentum distribution of the monitor events shown in Fig. 1 is in good agreement with the expected distribution of a Λ beam generated in K^--p interactions at rest (Table I). The number of K^--p events in flight is very small in this experiment. The half-width of the peak at 254 MeV/c in this distribution which arises from the reaction $K^-p\rightarrow\Lambda\pi^0$ is $\sim$5 MeV/c; the same width is also observed for the peak at 290 MeV/c which arises from the reaction $\Sigma^-p\rightarrow\Lambda n$ at rest. From the positions and widths of these peaks, the precision of the Λ-momentum measurement in this experiment is estimated to be $\sim$2%. This sample of Λ decay events was also used to measure the Λ lifetime, with the result $\tau_\Lambda = (2.45\pm0.06)\times10^{-10}$ sec.[7] The total Λ pathlength as function of the Λ momentum was then calculated by scaling up the pathlength observed for the monitor events to the total V^0 events found in the scan and properly taking into account the cutoff criteria.

[8] The weight $W(1)$ was calculated using the fact that the angular distribution of the decay proton in the Λ c.m. system is isotropic. $W(2)$, which is the weight corresponding to loss of events outside the fiducial volume and within 1 mm from the production point, was calculated using the Λ lifetime value of 2.45×10^{-10} sec. The weight $W(3)$ was calculated by assuming an isotropic distribution in space angles for all particles, namely, equal populations in each $\sin\lambda$ interval. In forming $W(3)$ we have also assumed that the dip angles of all tracks of each event are uncorrelated. This assumption has been tested on a sample of events and was found to be approximately correct. In those events where the total weight W ($=W_d$ or W_s) was larger than two times the average weight $W_{\rm av}(P)$ in the momentum region P (Fig. 4), we set $W=W_{\rm av}(P)$.

B. Scattering Events

The candidates for Λ-p scattering events found in the scan were measured and tried to be fitted by the THRESH and GRIND programs to the following reactions:

(1) $\Lambda+p\rightarrow\Lambda+p,\qquad \Lambda\rightarrow p+\pi^-;$

(2) $\bar{K}^0+p\rightarrow\Lambda+\pi^+,\qquad \Lambda\rightarrow p+\pi^-;$

(3) $K^0(\bar{K}^0)+p\rightarrow K^0(\bar{K}^0)+p,\quad K^0(\bar{K}^0)\rightarrow\pi^++\pi^-;$

(4) $\Lambda\rightarrow p+\pi^-$ (without interaction).

The fitting procedure for (1), (2), and (3) included also the V^0 production point in the K^--p and Σ^--p reactions. No ambiguity was found among reactions (1), (2), and (3). However, there were some events where the momentum transfer to the suspected recoil proton was so small that the events yielded good fits to both hypotheses (1) and (4). A rough calculation to estimate the number of scattering events due to background protons yielded an upper limit of $\sim$0.2% contamination in this experiment. Consequently, we have taken all the events which were ambiguous between hypotheses (1) and (4) as genuine Λ-p elastic scattering events.

On the fitted Λ-p elastic scattering events we have imposed cutoff values similar to those on the monitor events (a)-(d), namely, incoming momentum between 120 and 320 MeV/c; 1.0-mm space-length cutoff on the neutral-Λ pathlength before and after the scattering; 1.5-mm space-length cutoff on both recoil proton and Λ-decay proton; and dip cutoff at $\sin\lambda=0.98$ on all charged and neutral tracks. Following this cutoff procedure, a total of 378 events out of 603 fitted events remained for final analysis. The lower space-length cutoff $L_r=1.5$ mm for the recoil proton was derived from the study of the angular distribution of the scattered events shown in Fig. 5 as a function of the incident Λ momentum. The solid lines in this figure describe the lower limits of the Λ scattering angle corresponding to a cutoff on the recoil proton length of 1.0, 1.5, and 2.0 mm in space. As can be seen from Fig. 5,

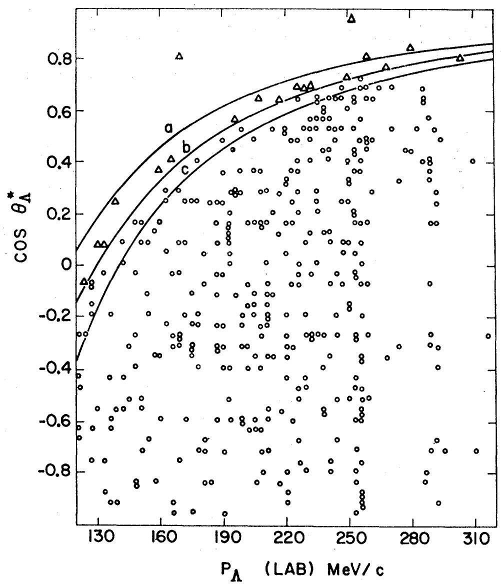

FIG. 5. Angular distribution of the scattering events in the c.m. system after imposing cutoffs (a)–(d) (see text) as a function of the Λ incoming momentum. The solid lines a, b, and c represent lower limits to the Λ scattering angle corresponding to space-length cutoffs on recoil proton of $L_r = 1.0$, 1.5, and 2.0 mm. Events above line b, which have been rejected in the final analysis, are represented by triangles.

the density of events is decreasing appreciably above the 1.5-mm line which for this reason was chosen as the cutoff value.

Following these cutoff criteria, a weight W' was assigned to every scattered event:

$$W' = W(1)\times W(2)\times W(2')\times W(3) = [P(1)\times P(2)\times P(2')\times P(3)]^{-1},$$

where $P(1)$ and $P(3)$ have the same meaning as in the case of the monitor events[8]; $P(2)$ and $P(2')$ are the probabilities for an event to satisfy the cutoff criterion on the neutral Λ track before and after the scattering. In forming the weight W' the weak correlations between $W(2)$, $W(2')$, and $W(3)$ were neglected.[9] In those cases where the number of events integrated over all scattering angles were of interest, such as in the total cross-section calculation, it was necessary to correct for the loss of small-angle scattering events corresponding to the recoil-proton cutoff. To this end an additional weight $W(4)$ was calculated, assuming an isotropic angular distribution of the scattered particles in the c.m. system of the Λ-p, which in turn yielded a total weight $W_s = W'\times W(4)$. Fortunately, the value of $W(4)$ is smaller in the higher-momentum regions where the isotropy assumption (S-wave scattering) might be less justified, and its main contribution is in the low-momentum region. The average weights per event W' and W_s as function of the Λ incident momentum are shown in Fig. 4.

C. Differential and Total Cross Sections

The Λ-p elastic scattering cross section as a function of the incident Λ momentum has been calculated for six intervals in the region 120–320 MeV/c. Two different momentum divisions have been considered: The first divided the region into equal momentum intervals and the second into intervals with approximately the same number of events. Cross-section values for both divisions are given in Table II. The behavior of the total cross section as a function of momentum appears to be smoother in the second division method, while in the first there seems to be some shoulder in the region 180–210 MeV/c which, however, most probably is just statistical fluctuation. The dependence of the cross section on the cutoff values adopted has been examined. As can be seen from Table III, the cross-section values are almost independent of the cutoff values and their small variations are well within the experimental statistical errors. The results also turned out to be insensitive to variation in the fiducial volume.

The Λ-p differential elastic scattering cross section is represented in Fig. 6 for six momentum intervals, where each event is represented by its weight W' defined earlier. As can be seen in this figure, the angular distribution of the scattering events is essentially isotropic in the whole momentum region 120–320 MeV/c, which in turn means that the elastic scattering cross section is consistent with a predominantly S-wave scattering. The angular distribution cannot be analyzed

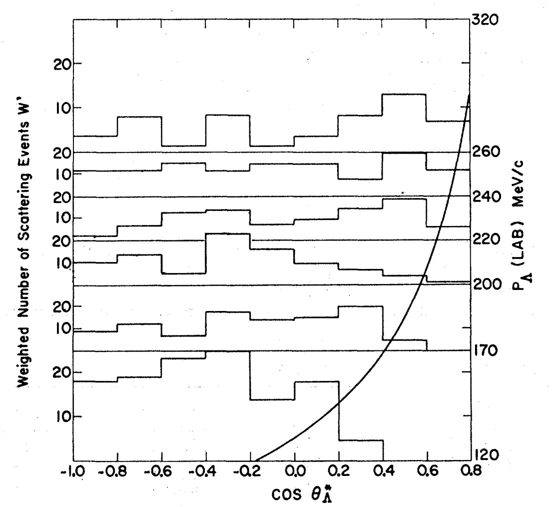

FIG. 6. Angular distribution of the scattering events after imposing the cutoff criteria in various momentum intervals, where each event is weighted by W' (see text). The solid line represents the lower limit of the Λ-scattering angle corresponding to a space-length cutoff of 1.5 mm on the recoil proton.

[9] In fact an evaluation of the cross section with a sample of about $\frac{2}{3}$ of the present statistics, taking into account all correlations, yielded essentially the same values as in this paper, which means that the correlations average out. [G. Zech, thesis for troisiéme cycle, Faculté des Science, Université de Strasbourg, 1966 (unpublished).]

TABLE II. Λ-p total and differential elastic cross sections in two different momentum divisions (see text). F/B stands for the forward-to-backward ratio and P/E for the polar-to-equatorial ratio. The polarization $\alpha\bar{P}(\theta_\Lambda{}^*)$ of the outgoing Λ averaged over two regions of production angles is also presented, where α is the Λ-decay asymmetry parameter.

Momentum interval (MeV/c)	No. of events	Cross section (mb)	Angular distribution F/B	P/E	Polarization $\alpha\bar{P}(\theta_\Lambda{}^*)$ $-1<\cos\theta_\Lambda{}^*<0$	$0<\cos\theta_\Lambda{}^*<1$
120–150	34	212±36	...	...	...	...
150–180	48	141±20	...	...	...	...
180–210	80	141±16	1.01±0.24	0.87±0.22	−0.16±0.28	−0.40±0.36
210–240	88	95±10	1.27±0.28	0.79±0.19	−0.10±0.31	−0.17±0.29
240–270	92	81± 8	1.29±0.27	1.12±0.24	0.42±0.30	−0.45±0.28
270–320	36	56± 9	1.55±0.53	0.99±0.34	0.29±0.53	0.0 ±0.43
120–170	65	180±22	...	...	...	...
170–200	62	130±17	...	...	...	...
200–220	58	118±16	0.55±0.16	1.00±0.29	0.0 ±0.31	−0.50±0.48
220–240	65	101±12	1.76±0.45	0.74±0.20	−0.37±0.38	−0.11±0.32
240–260	85	83± 9	1.16±0.25	1.14±0.25	0.48±0.30	−0.51±0.29
260–320	43	57± 9	1.92±0.62	1.01±0.32	0.13±0.52	0.0 ±0.38

in detail in the present experiment, because the number of events per momentum interval per scattering angle is quite small. The two ratios of the angular distribution, forward to backward (F/B) and polar to equatorial (P/E), are given in Table II for the higher incident-Λ momentum intervals where the corrections due to the various cutoffs are small. In calculating the quantities F/B and P/E, we have corrected for events lost due to the short recoil-proton cutoff by assuming that the differential cross section is isotropic in F and in P, respectively. The behavior of the quantity F/B is more regular and centered around unity in the first momentum-division method. However, in both division methods there is a small tendency towards $F/B>1$ for the higher-momentum intervals.

Finally, we have searched for possible polarization effect in the Λ-p low-energy elastic scattering. Figure 7 presents the distribution of the quantity $\cos\theta_\pi=\mathbf{n}_\pi\cdot\mathbf{n}_s/|\mathbf{n}_\pi||\mathbf{n}_s|$ as function of the scattering angle $\theta_\Lambda{}^*$, where $\mathbf{n}_\pi$ is a vector in the direction of the decaying π^- in the Λ c.m. system and $\mathbf{n}_s$ is the normal to the scattering plane. Figure 7 illustrates the fact that the polarization is consistent with zero for all scattering $\theta_\Lambda{}^*$ angles. This fact is also shown in Table II, where the average polarization $\alpha\bar{P}(\theta_\Lambda{}^*)$ is given, α being the asymmetry parameter of the Λ decay.

III. LOW-ENERGY Λ-p SCATTERING PARAMETERS

As shown previously, both the angular distribution and the polarization indicate that the Λ-p elastic scattering in the momentum region 120–320 MeV/c is consistent with S-wave scattering dominance. This fact may be further substantiated through the semiclassical argument that the highest partial wave $l_{\max}$ participating in the interaction is given by the expression $l_{\max}\leq kR$, where k is the wave number and R is the interaction radius. Assuming the two-pion-exchange (TPE) mechanism to be responsible for the longest interaction range of the Λ-p system, one obtains the value of $R\sim1.5$ F. Thus at the upper end of the Λ-momentum range of this experiment (320 MeV/c), $l_{\max}\leq1.1$, which means that the scattering takes place predominantly in S-wave through the whole momentum region.

The energy dependence of the singlet and triplet S-wave phase shifts is given in the effective-range formalism, neglecting the shape-dependent term, as

$$k\cot\delta_{s,t}=-1/a_{s,t}+0.5r_{s,t}k^2\,, \qquad (3.1)$$

where a is the scattering length, r is the effective range, and s, t stand for singlet and triplet states. From this expression the total elastic scattering cross section is

TABLE III. Total Λ-p cross section obtained with various cutoff values, changing one cutoff at a time and leaving the other values as used in this paper. L_0, L_d, and L_r are lower cutoffs on the length of the neutral Λ, the decay proton, and the recoil proton, respectively. λ is the upper cutoff on the dip angle.

Varied cutoff (lengths in mm)	No. of events	Cross section (mb) for various momentum intervals (MeV/c) 120–170	170–200	200–220	220–240	240–260	260–320
Ordinary cutoffs	378	180±22	130±17	118±16	101±12	83± 9	57± 9
$L_0=1.5$	348	184±24	128±17	122±17	100±13	85±10	60± 9
$L_0=2.0$	324	173±25	135±18	121±17	97±13	92±10	61±10
$L_d=1.0$	391	175±21	136±17	119±15	99±12	81± 9	57± 9
$L_d=2.0$	368	185±23	132±17	121±16	100±13	82± 9	56± 9
$L_r=1.0$	391	172±20	124±16	114±15	99±12	82± 9	57± 9
$L_r=2.0$	355	163±23	131±17	121±16	102±13	82± 9	56± 9
$\sin\lambda=0.96$	347	187±24	134±18	122±16	95±13	83± 9	55± 9
$\sin\lambda=0.94$	328	201±26	136±19	124±17	101±14	85±10	58±10
$\sin\lambda=0.92$	294	201±27	134±19	132±19	93±14	85±11	51± 9

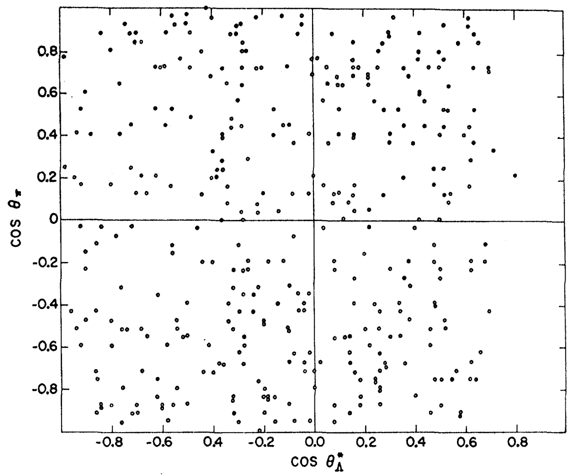

FIG. 7. Angular distribution of the decaying π meson with respect to the normal to the scattering plane as a function of the Λ-scattering angle.

given by

$$\sigma=\tfrac{1}{4}\sigma_s+\tfrac{3}{4}\sigma_t=\frac{\pi}{k^2+(-1/a_s+0.5r_sk^2)^2}+\frac{3\pi}{k^2+(-1/a_t+0.5r_tk^2)^2}. \quad (3.2)$$

The experimental Λ-$p\rightarrow\Lambda$-p cross sections have been fitted by using the maximum-likelihood method with Eq. (3.2), taking a_s, a_t, r_s, and r_t as free parameters, and also in the zero-range approximation ($r_s=r_t=0$). The best fits have been obtained by maximizing the likelihood functions $L(a_s,a_t,r_s,r_t)$ and $L(a_s,a_t,0,0)$, respectively. In order to obtain fits sensitive to the detailed variation of the cross section with momentum, the experimental values have been taken in 10-MeV/c intervals in the momentum range 120–320 MeV/c. The best values for the four-parameter fit are shown in Table IV for several momentum regions (see also Fig. 8). The zero-range approximation ($r_s=r_t=0$) yielded for the likelihood function $L_{\max}(a_s,a_t,0,0)$ a value considerably lower than the function $L_{\max}(a_s,a_t,r_s,r_t)$. No errors are quoted for the best-fitted values in Table IV since there is a strong correlation between the scattering

TABLE IV. Four-parameter fits of the Λ-p scattering data for various momentum intervals.

Momentum range P_Λ (MeV/c)	a_s (F)	a_t (F)	r_s (F)	r_t (F)
120–320	−1.8	−1.6	2.8	3.3
140–320	−1.6	−1.4	2.7	2.4
160–320	−1.7	−1.6	2.8	3.1
120–300	−2.3	−1.4	3.0	2.9
120–280	−3.6	−1.1	3.7	1.6
120–260	−1.3	−1.6	3.3	2.6
120–240	−1.4	−1.6	3.1	2.6

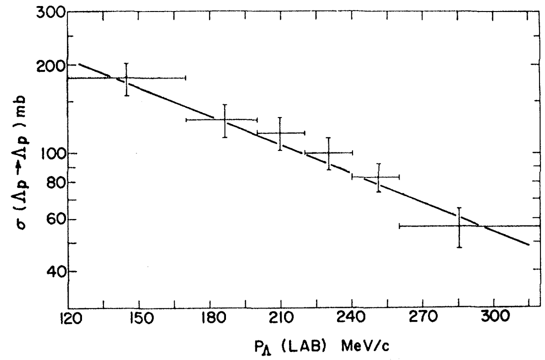

FIG. 8. Λ-proton elastic scattering cross sections. The solid line represents the best fit to the experimental data obtained from a four-parameter fit in the effective-range formalism.

parameters indicated by the large off-diagonal elements in the error matrix. Instead, the significance of the best scattering-length parameters is illustrated through a mapping of the likelihood function L in an a_s-a_t plane (Fig. 9). For each point in the plane, the maximal value of L was calculated varying r_s and r_t independently in a reasonable range of 1–5 F. Note that this mapping procedure yields upper limits to the error domain of the best a_s and a_t values. In Fig. 9 are also shown early calculations of scattering lengths derived from hypernuclei data.[10–12] Most of the hypernuclei points lie in the region of more than one standard deviation from the best values obtained in this experiment. From general spin considerations of light hypernuclei it was

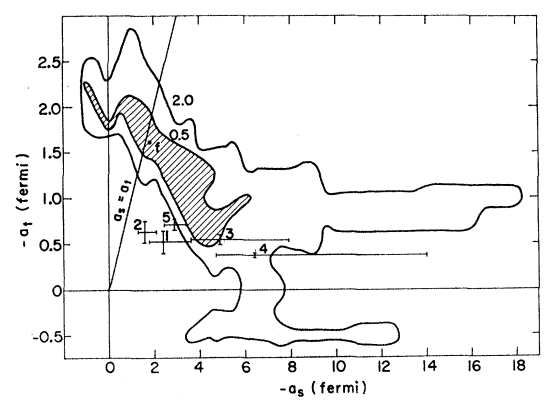

FIG. 9. Mapping of the likelihood function L in the a_s-a_t plane for the four-parameter fit. The shaded area includes all points with likelihood values above $L_{\max}$/exp0.5, where $L_{\max}$ is the value of the best fit (point f). The external smooth curve encloses likelihood values lying above $L_{\max}$/exp2.0. Points 1–5 represent scattering lengths derived from early hypernuclei calculations. (See Refs. 10–12.)

[10] B. W. Downs and R. H. Dalitz, Phys. Rev. **114**, 593 (1959).
[11] K. Dietrich, H. J. Mang, and R. Folk, Nucl. Phys. **50**, 177 (1964).
[12] R. C. Herndon, Y. C. Tang, and E. W. Schmid, Phys. Rev. **137**, B294 (1965). Recent calculations, partially based on our earlier results, yielded better agreement between hypernuclei predictions and scattering results; see R. C. Herndon and Y. C. Tang, Phys. Rev. **153**, 1091 (1967); **159**, 853 (1967); **165**, 1093 (1968).

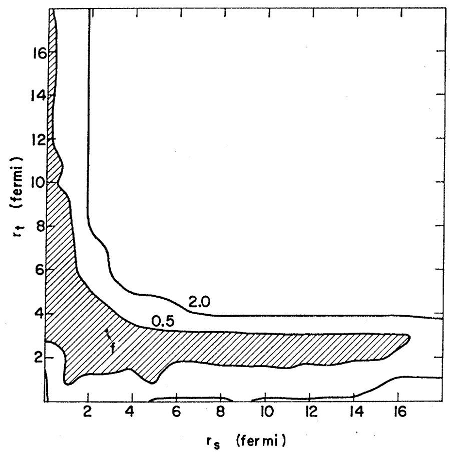

FIG. 10. Mapping of the likelihood function L in the r_s-r_t plane for the four-parameter fit. The shaded area, the external smooth curve, and the point f have the same meaning as in Fig. 9.

deduced that $|a_s| \geq |a_t|$,[1] which reduces the domain lying inside one standard deviation (Fig. 9).

A similar likelihood mapping is presented for the r_s-r_t plane (Fig. 10), where L is maximized by varying independently a_s between -6 and $+1$ F and a_t between -2.25 and -0.5 F. These variation limits were chosen as roughly representing the one-standard-deviation domain in the a_s-a_t plane.

The relatively large region of a_s, a_t values, which are still consistent with the experimental data within one standard deviation, may be reduced by the introduction of further assumptions on the nature of the scattering. The effective range r can be expressed in terms of the intrinsic range b and the scattering length a through the relation[13,14]

$$r = b(1 - Q(s)b/a)\,, \tag{3.3}$$

where Q is a function of the well-depth parameter s. For negative values of a_s and a_t, Q is essentially independent of s in the allowed region of $0<s<1$, but changes with the potential shape. For simple central potentials, Q has the following values[14]:

$$\begin{aligned} &Q \simeq 0.5, \text{ Gaussian potential;} \\ &Q \simeq 0.65, \text{ exponential potential;} \\ &Q \simeq 0.9, \text{ Yukawa potential.} \end{aligned} \tag{3.4}$$

Under the assumption that the singlet and triplet intrinsic ranges are equal ($b_s = b_t = b$) and using relation (3.3), a three-parameter fit to the experimental data has been carried out by taking a_s, a_t, and b as free variables. The results are presented in Table V for the three values of Q given in (3.4). The fitted values obtained for a_s, a_t, and b are rather insensitive to the potential shape Q, yielding a relatively high value for the intrinsic range b of $\sim$1.8 F. The values obtained for a_s and a_t are similar to the ones obtained in the four-parameter fits.

Two-parameter fits have also been performed with a_s and a_t as free parameters. Characteristic values of Q (0.5, 0.65, 0.9) have been used with an average value of $b = 1.8$ F. Another set of fits have been carried out for an average value of $Q = 0.7$ and several values of the intrinsic range b: 0.84 F, corresponding to one-kaon exchange (OKE); 1.5 F, corresponding to TPE; 1.7 F, 1.9 F, and 2.1 F. The results of these fits which are presented in Table V, do not depend critically on the potential shape Q; on the other hand, they are relatively strongly dependent on the intrinsic range b. The best values of r_s for $b = 1.5$ and 2.1 F with $Q = 0.7$ are unphysical; however, the domain of one standard deviation encloses also reasonable r_s values.

The likelihood function mappings in the a_s-a_t plane for the two-parameter fits with $Q = 0.7$ and various values of b are presented in Fig. 11. As expected, these mappings show that the one-standard-deviation domain has been considerably shrunk in comparison to the four-parameter fit. Also seen from Table V and Fig. 11 is the tendency of $|a_s|$ to decrease and of $|a_t|$ to increase with larger values of b.

A relation between the effective range, the scattering

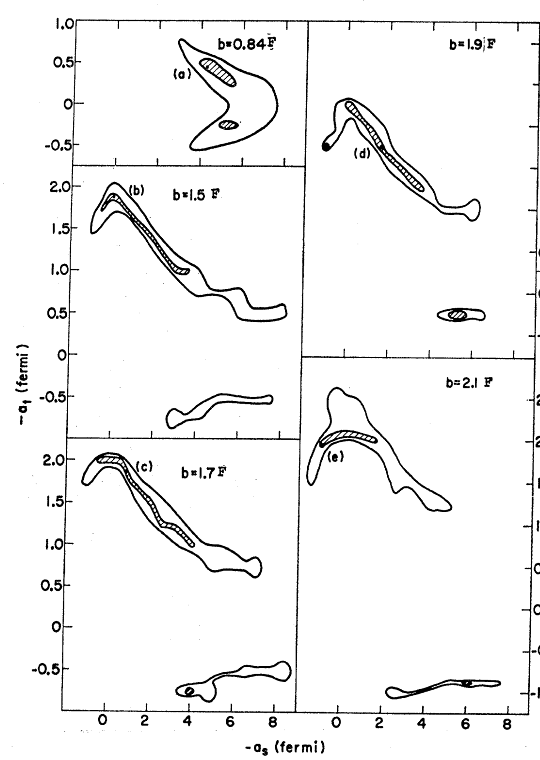

FIG. 11. Mapping of the likelihood function L in the a_s-a_t plane for the two-parameter fits with a_s, a_t as free parameters and r_s, r_t given by (3.3) for various b values and for an average value of $Q = 0.7$. The shaded areas and the external smooth curves have the same meaning as in Fig. 9. Points (a)-(e) represent the best-fit values.

[13] J. J. de Swart and C. Dullemond, Ann. Phys. (N.Y.) **19**, 458 (1962).

[14] R. D. Levee and R. L. Pexton, Nucl. Phys. **55**, 34 (1964).

TABLE V. Three- and two-parameter fits of the Λ-p scattering data. The effective range r is expressed in terms of the intrinsic range b and the scattering length a via the relation (3.3). For each fit the logarithm of the likelihood function L corresponding to the best values of the scattering parameters is also given.

Free parameters	$Q(s)$	Intrinsic range b (F)	a_s (F)	a_t (F)	r_s (F)	r_t (F)	$-\ln L_{max}$
a_s, a_t, b	0.5	2.0	−1.5	−1.7	3.3	3.1	50.57
	0.65	1.8	−1.3	−1.8	3.5	3.0	50.57
	0.9	1.6	−1.2	−1.8	3.7	3.0	50.58
a_s, a_t	0.5	1.8	−0.5	−1.9	5.4	2.6	50.59
	0.65	1.8	−1.8	−1.6	3.0	3.1	50.58
	0.9	1.8	−1.7	−1.8	3.6	3.4	50.69
	0.7	0.84	−4.3	−0.5	1.0	1.9	50.86
	0.7	1.5	0.0	−1.9	∞	2.3	50.65
	0.7	1.7	−0.8	−1.9	4.2	2.8	50.59
	0.7	1.9	−1.7	−1.8	3.4	3.4	50.63
	0.7	2.1	+1.0	−2.0	−1.0	3.7	50.65

length, and the shape-dependent parameter P in the expression

$$k\cot\delta = -1/a + 0.5rk^2 - Pr^3k^4 \tag{3.5}$$

has been derived by Dosch and Müller.[15] Their relation is based on a dynamical model using a subtracted partial-wave dispersion relation where the left-hand cut is determined by a one-boson-exchange mechanism. The essential contribution to this process is given by an exchange of an effective scalar meson ($I=0$; $J^P=0^+$) which appears to be of importance also in N-N scattering. Using the Dosch-Müller relation in the form

$$\begin{aligned} r_s &= 2.0 - 3.1(1/a_s) + 1.4(1/a_s)^2 \\ &\quad + 0.08(1/a_s)^3 - 0.03(1/a_s)^4, \\ &\qquad (-0.03 < P_s < -0.01) \end{aligned} \tag{3.6}$$

$$\begin{aligned} r_t &= 2.0 - 3.0(1/a_t) + 1.1(1/a_t)^2 \\ &\quad + 0.09(1/a_t)^3 - 0.03(1/a_t)^4, \\ &\qquad (-0.03 < P_t < -0.015) \end{aligned}$$

and setting $P_s = P_t = -0.02$, we have performed a two-parameter fit to the experimental data with the results $a_s = -2.16$ F, $a_t = -2.10$ F, $r_s = 3.72$ F, and $r_t = 3.67$ F. Although our data are not sensitive to the parameter P, we have used in this last fit the expression (3.5) to be able to use the Dosch-Müller relation in full.

The last interesting relation considered in this work was the one derived from $SU(6)$ symmetry,[16] namely,

$$a_s(\Lambda - p) = a_t(\Lambda - p). \tag{3.7}$$

It is well known that symmetry-derived relations between reactions are expected to hold mainly at high energies where the symmetry-breaking terms should be small. However, if there is any meaning at all to symmetry-reaction relations at low energy, they should be tested for the Y-N system where, contrary to the N-N interaction,[17] no bound state is so far known that could break the symmetry. The best values of a_s and a_t obtained in this experiment are not in disagreement with relation (3.7).

IV. DISCUSSION AND CONCLUSIONS

Preliminary results of a similar experiment on low-energy Λ-p elastic scattering between 120 and 330 MeV/c have been reported by the Maryland group,[3,18] using somewhat different cutoff criteria and weighting procedures. The total elastic scattering cross sections of the Maryland group are essentially identical with the ones reported here.[2] The cross-section behavior as a function of the incident momentum of both experiments does not seem to support the possible existence of a low-energy Λ-p excited state such as the one at the mass 2058±8 MeV discussed by Melissinos *et al.*[19] The small enhancement observed in our total Λ-p cross section (Table II) is with the present statistics dependent on the momentum division and might well be due to statistical fluctuation.

The differential elastic scattering cross section of the Maryland group is also in good agreement with the one reported here. The F/B ratio is essentially equal to 1 in the momentum region under investigation, with a small tendency to increase at the upper end of the momentum. However, the deviation from an isotropic angular distribution is small and still consistent with a predominantly S-wave scattering. The possible existence of a P-wave contribution to the elastic scattering at the upper end of the momentum region does not change by more than one standard deviation the scattering parameters calculated in this experiment (Table IV and Fig. 9). At the same time, the insensitivity of the best

[15] H. G. Dosch and V. F. Müller, Nuovo Cimento **39**, 886 (1965); Phys. Letters **19**, 320 (1965); and (private communication).

[16] D. A. Akyeampong and R. Delbourgo, Phys. Rev. **140**, B1013 (1965); V. Barger and M. H. Rubin, *ibid.* **140**, B1366 (1965); Y. Frishman (private communication).

[17] The $SU(6)$ prediction for the N-N scattering lengths, $a_s(n-p) = a_t(n-p)$, is strongly violated, probably due to the existence of bound states.

[18] B. Sechi-Zorn, R. A. Burnstein, T. B. Day, B. Kehoe, and G. Snow, Phys. Rev. Letters **13**, 282 (1964); R. A. Burnstein, University of Maryland, Technical Report No. 469, 1965 (unpublished); B. Sechi-Zorn, B. Kehoe, J. Twitty, and R. A. Burnstein, University of Maryland, Technical Report No. 846, 1968 (unpublished).

[19] A. C. Melissinos, N. W. Reay, J. T. Reed, T. Yamanouchi, E. Sacharidis, S. J. Lindenbaum, S. Ozaki, and L. C. L. Yuan, Phys. Rev. Letters **14**, 604 (1965).

values to the low-momentum cutoff has been verified (Table IV).

The spin dependence of the Λ-p interaction as derived from the elastic scattering experiment ($a_s/a_t \gtrsim 1$) seems to be weaker than what was indicated from early hypernuclei calculations ($a_s/a_t \gtrsim 4$).[1,13] The singlet scattering length which is mainly derived from the simple hypernucleus $_\Lambda H^3$ is in good agreement with the one obtained in this experiment. On the other hand, the triplet scattering length derived in hypernuclei calculations mainly from $_\Lambda He^5$ seems to be underestimated. Recently several explanations for this discrepancy have been suggested: (1) A strong tensor force in the Λ-N system will influence less the Λ-α system and will cause a reduction in the over-all $_\Lambda He^5$ interaction potential.[1] (2) A repulsive three-body force will affect the $_\Lambda He^5$ hypernucleus more than the $_\Lambda H^3$ hypernucleus and will consequently reduce the over-all attraction in the $_\Lambda He^5$.[1,20] (3) The TPE diagram which mainly contributes to the triplet Λ-N force through the intermediate Σ-N state is suppressed in the Λ-α system, since the lowest allowed intermediate state involves the excited state of He^4. This will reduce the contribution to the triplet potential in $_\Lambda He^5$.[21] (4) The possible existence of a spin-flip transition in the $_\Lambda H^3$ will reduce the spin dependence of the Λ-N interaction and shift the scattering parameters values nearer to the ones obtained in this experiment.[21] (5) The possible existence of a symmetry-breaking part in the Λ-N potential[22] may explain the difference between the scattering-length values derived from Λ-p elastic scattering and those from hypernuclei data where charge symmetry was assumed. This symmetry-breaking assumption may be tested through a comparison between the Λ-p and Λ-n systems in final-state interactions or in low-energy Λ-d scattering.

[20] A. R. Bodmer and S. Sampanthar, Nucl. Phys. **31**, 251 (1962); A. R. Bodmer and J. W. Murphy, *ibid.* **64**, 593 (1965); A. Gal, Phys. Rev. **152**, 975 (1966).

[21] A. R. Bodmer, Phys. Rev. **141**, 1387 (1966).

[22] B. W. Downs and R. J. N. Phillips, Nuovo Cimento **41**, 374 (1966).

Since the low-energy scattering parameters are insensitive to the Λ-N potential shape, no information can be derived from this scattering experiment on the details of the potential (Table V). On the other hand, the scattering parameters are dependent on the range of the potential. From the hypernuclei data no conclusion could be derived on the range of the Λ-N forces and it has been fixed arbitrarily to that of a TPE ($b = 1.5$ F) or OKE ($b = 0.84$ F). The best b value of the present experiment is consistent with a somewhat larger intrinsic range ($b \simeq 1.8$ F). If indeed the intrinsic range is higher than the TPE value, it may be explained by a dominant contribution to the potential from boson exchange with a mass lower than the mass of two pions, namely, around 230 MeV. So far such a boson has not been found experimentally although the exchange of low-mass scalar bosons have been considered in various Λ-N potential calculations.[15,23] A more reasonable explanation is the existence of a repulsive hard core in the Λ-N potential. The inclusion of a hard core has also been considered in various hypernuclei calculations, in analogy to the N-N system, where its existence is well established. The over-all intrinsic range b is related to the intrinsic range of the attractive part b_0 by[24] $b_0 = b - 2d$, where d is the hard-core radius. Consequently, nonzero d values would increase the apparent values of b. In this connection it is worth while to note that an upper limit of $d \cong 0.6$ F is deduced from the absence of a bound hyperdeuteron.[1]

ACKNOWLEDGMENTS

We would like to thank J. M. Blatt, R. H. Dalitz, H. G. Dosch, A. Gal, and G. Zech for helpful discussions and comments. We would like also to acknowledge the participation of O. Benary, A. Fridman, A. Minguzzi-Ranzi, and B. Schiby in the early stages of this experiment.

[23] B. W. Downs and R. J. N. Phillips, Nuovo Cimento **33**, 137 (1964); **36**, 120 (1965).

[24] T. Ohmura, M. Morita, and M. Yamada, Progr. Theoret. Phys. (Kyoto) **15**, 222 (1956).